Climate Dynamics (2000) 16:35–48

H.-H. Syu · J. D. Neelin

ENSO in a hybrid coupled model. Part II: prediction with piggyback data assimilation

Received: 17 April 1998 / Accepted: 22 July 1999

Abstract A hybrid coupled model (HCM) for the tropical Pacific ocean-atmosphere system is employed for ENSO prediction. The HCM consists of the Geophysical Fluid Dynamics Laboratory ocean general circulation model and an empirical atmospheric model. In hindcast experiments, a correlation skill competitive to other prediction models is obtained, so we use this system to examine the effects of several initialization schemes on ENSO prediction. Initialization with wind stress data and initialization with wind stress reconstructed from SST using the atmospheric model give comparable skill levels. In re-estimating the atmospheric model in order to prevent hindcast-period wind information from entering through empirical atmospheric model, we note some sensitivity to the estimation data set, but this is considered to have limited impact for ENSO prediction purposes. Examination of subsurface heat content anomalies in these cases and a case forced only by the difference between observed and reconstructed winds suggests that at the current level of prediction skill, the crucial wind components for initialization are those associated with the slow ENSO mode, rather than with atmospheric internal variability. A "piggyback" suboptimal data assimilation is tested in which the Climate Prediction Center data assimilation product from a related ocean model is used to correct the ocean initial thermal field. This yields improved skill, suggesting that not all ENSO prediction systems need to invest in costly data assimilation efforts, provided the prediction and assimilation models are sufficiently close.

H.-H. Syu
Jet Propulsion Laboratory,
California Institute of Technology, Pasadena,
CA 91109, USA

J. D. Neelin (✉)
Department of Atmospheric Sciences,
University of California, Los Angeles,
Los Angeles, CA 90095, USA
E-mail: neelin@atmos.ucla.edu

1 Introduction

The El Niño/Southern Oscillation (ENSO) phenomenon is the strongest climate variation on an interannual time scale, originating from tropical ocean-atmosphere system but having a global impact on weather patterns. The ENSO phenomenon demonstrates a quasi-periodic/cyclic behavior, which implies a potential predictability for ENSO. Several prediction schemes have been developed over the past years, including statistical models (e.g., Xu and von Storch 1990; Barnston and Ropelewski 1992; Jiang et al. 1995) and physical coupled models, including intermediate models (e.g., Cane et al. 1986), hybrid coupled models (Latif and Flügel 1991; Barnett et al. 1993) and coupled general circulation models (GCMs) (e.g., Latif et al. 1993; Ji et al. 1994). Reasonable forecasts are now possible up to one year or so in advance. Further examples are noted in a review paper by Latif et al. (1998). Among these models, the Cane and Zebiak model (1985, 1987, CZ model hereafter), an intermediate model, was the first coupled model used for ENSO prediction and demonstrated significant skill in predicting the equatorial sea surface temperature (SST) anomalies at lead times beyond one year. Latif and Flügel (1991) were the first to use an empirical atmospheric model in coupled prediction experiments. They used an ocean GCM (OGCM) coupled to an extremely simple empirical feedback model in which the anomalous surface wind stress at a given grid point was expressed only in terms of the local SST anomaly. Barnett et al. (1993) also coupled an OGCM to an empirical atmospheric model, calculated by canonical analysis, at the same level of complexity as the hybrid coupled model (HCM) considered here (Syu et al. 1995; Syu and Neelin 1999, part I hereafter).

Although ENSO has a tendency to cyclic behavior, the observed NINO3 indices (averaged SST anomaly from 5°N–5°S and 150–90°W) show that ENSO extremes occur irregularly both in time and amplitudes. Hypotheses for ENSO irregularity include (1) deter-

ministic chaos within the slow components of the coupled system (Jin et al. 1994, 1996; Tziperman et al. 1994, 1995; Chang et al. 1994, 1995), and (2) stochastic forcing by "weather noise" (Kleeman and Power 1994; Kleeman and Moore 1997; Jin et al. 1996; Blanke et al. 1997; Eckert and Latif 1997). Weather noise refers to the effects of atmospheric variability that has relatively short decorrelation times, and thus may be approximated as random on ENSO time scales. In the HCM used here, chaos produces only slight irregularity (part I), and thus weather noise would be the default hypothesis.

Since ENSO irregularity might be attributed to intrinsic chaos and weather noise, ENSO predictability may be limited by these two factors. In addition, it may also be attributed to the initialization procedure for ENSO prediction experiments (Cane et al. 1986; Latif et al. 1993; Chen et al. 1995). The growth of initial error is discussed in works such as Goswami and Shukla (1991), Blumenthal (1991), and Penland and Sardeshmukh (1995). Goswami and Shukla (1991), using the CZ model, found that the growth of small initial error is governed by processes with two time scales, with doubling times of 5 months and 15 months, respectively. A similar initial growth rate of 6 months, based on seasonality, is suggested in Blumenthal (1991). He showed that for a system which is not self-adjoint, initial error could grow in a mode that is not a growing normal mode of classical stability analysis. Penland and Sardeshmukh (1995) suggested that the rapid growth of initial error can be associated with constructive interactions between several damped non-normal modes after an optimal initial structure is set up by white noise. Effects of initial errors on ENSO prediction may be reduced by data assimilation schemes (Hao and Ghil 1994; Ji et al. 1995; Fischer et al. 1995), specifically in the upper-ocean thermal structure (Xue et al. 1994; Ji et al. 1994, 1995; Fischer et al. 1995). Recent studies indicate the benefits of data assimilation on coupled model prediction skill (Ji et al. 1996; Ji and Leetmaa 1997; Rosati et al. 1997). In this study, we consider the impact of using a data assimilation product from a related but not identical system on ENSO prediction. This procedure is suboptimal but cheaper than redoing the data assimilation for each model system. We consider other initialization schemes to help quantify the effects of SST and ocean sub-surface memory in predictability. We also attempt to estimate the impact of atmospheric internal variability ("weather noise") on ocean initial conditions compared to the wind feedback associated with the past history of SST.

In part I of this two-part study, the HCM simulation of ENSO is described. The HCM is closely related to that of Syu et al. (1995). The empirical atmospheric model is estimated from the covariance of the observed sea surface temperature and wind stress anomalies using a singular value decomposition (SVD) method (see Syu et al. 1995 for details). The effects of physical processes, specifically the ocean vertical mixing schemes and the atmospheric spin-up time, on simulated ENSO periods are examined. A standard version of the HCM is defined in part I. The coupled behavior with the standard version exhibits realistic spatial and temporal structures, with periods of 3 to 4 years. Here, the model described in part I is employed for ENSO predictability studies and to discuss implications of various initialization schemes for ENSO prediction. Real-time predictions with this system have been described in Syu and Neelin (1997). We note that no "MOS" (model output statistics) correction is used in the model, that is, no statistically constructed correction between model fields and observations is used at any stage. This differs, for instance, from Barnett et al. (1993), in which such correction is used within the coupling (e.g., to get MOS-corrected SST from model SST before coupling to the atmosphere).

The work is organized as follows. Section 2 introduces data and methods used in prediction experiments. The sensitivity of the atmospheric component of the hybrid coupled model is addressed in Sect. 3. Section 4 describes the initial fields for hindcast experiments. Assessment of HCM ENSO prediction and effect of initialization schemes is carried out in Sect. 5. Conclusions are given in Sect. 6.

2 Data and method

Several initialization schemes are applied. The first initialization scheme is the widely used Cane et al. (1986) initialization scheme, in which the coupled model is initialized by the model ocean field that is forced by observed wind stress. Since the only given information is wind stress in the initialization, this scheme is referred to as the "stress-only" scheme. We use the Florida State University (FSU) converted wind stress (Legler and O'Brien 1984) time series from 1976 to 1993, with the drag coefficient of 1.2×10^{-3}, to integrate the ocean model up to the beginning hindcast time to initialize the ocean memory.

The second initialization scheme makes use of the ocean model data assimilation product from the Climate Prediction Center (CPC) (Ji et al. 1995). In addition to the specified FSU wind forcing, the CPC reanalyzed anomalous temperature field is "injected" into the ocean model (27 layers) every month since 1980 up to the beginning of the hindcast time. The scheme is hereafter referred to as the "injection" scheme. Because our ocean model (GFDL modular ocean model) is reasonably close to the one used by CPC, consistency is assumed in using the CPC reanalyzed data for our data assimilation purposes. It is necessary to make a distinction between this procedure and raw-data injection. We thus also refer to it as a piggyback data assimilation scheme, because it makes use of the effort from the CPC data assimilation system. This suboptimal piggyback data assimilation scheme, if it works, may point to the possibility that not every model needs to redo its own data assimilation if the chosen data assimilation product is appropriate.

In both schemes mentioned, observed wind stress is used in initializing the ocean fields. The observed wind data contains a component associated with the slow ENSO mode that can be explained by SST variation and also a component that cannot be explained by SST, including weather noise and errors. The weather noise can be important in exciting the ENSO mode or contributing to its irregularity (Kleeman and Power 1994; Penland and Sardeshmukh 1995; Blanke et al. 1997; Eckert and Latif 1997). However, observations also include errors due to measurement. In the third initialization scheme, we use the SVD reconstructed wind stress anomalies, instead of the observed FSU wind anomalies, to force the uncoupled OGCM. This scheme is used in Barnett et al.

(1993). Note that only observed SST information is used in this scheme, through a reconstructed wind field (stress from SST), to obtain the initial field. This initialization scheme is therefore referred to as the "stress-from-SST" scheme. To estimate if the weather noise information contained in the FSU wind data is significant enough to overcome the additional source of error, we compare the model results given by the FSU wind forcing and the reconstructed wind forcing. The reconstructed SVD wind stress is obtained by projecting the observed Reynolds' SST (Reynolds 1988) anomalies from 1976 to 1993 to the SVD model, representing the portion of wind associated with the ENSO mode that can be explained by SST. The residual wind between the FSU wind and reconstructed wind thus represents a combination of atmospheric internal variability, or weather noise and errors. This weather noise product is assessed quantitatively by Blanke et al. (1997) and confirmed to have a short decorrelation time.

The last initialization scheme is the "inject-SST" scheme. In this scheme, in addition to the FSU stress forcing, the Reynolds' SST anomaly information is injected into the first three ocean model layers on a daily basis. In the "injection" scheme, both SST and ocean sub-surface information are corrected. By comparing the difference between the injection scheme and the inject-SST scheme, the impact of the ocean sub-surface memory can thus be quantified.

Hindcast experiments are carried out up to 24 months from the initialized ocean fields by a version of the coupled model, which includes the surface-layer parametrization and 60-day atmospheric spin-up time scale (please refer to part I). The ocean climatology used in all hindcast experiments is specified to be the averaged model SST, forced by FSU wind stress over 1978 to 1993 without modification by the data assimilation scheme, i.e., the stress-only uncoupled simulation. The climatological wind stress used in the hindcast experiment is also specified to be the average of the FSU wind stress over the same period (1978–1993). The hindcast result will be verified against the observed data from the Reynolds' SST data set (Reynolds 1988).

Since the SVD atmospheric model is estimated from the observed data from 1970–1988, we need to re-estimate a set of the SVD models which excludes the period that overlaps with the hindcast period. For example, when period 1981–83 is being hindcast, the SVD model used is obtained from the observations of 1970–1980 and 1984–1988. Thus, no observations from the hindcast period have entered the model through SVD reconstructed winds in any hindcast experiment. Another series of hindcast experiments with a fixed SVD model that is used in ENSO simulations, in which the hindcast-period data are not removed, will also be carried out for comparison.

3 Sensitivity to SVD model estimation

As indicated in part I, coupled periods and amplitudes are sensitive not only to the change of ocean vertical mixing scheme and the atmospheric spin-up time, but also to the slightly different SVD models used in part I and Syu et al. (1995). In the hindcast experiments presented here, a set of SVD models are used which are derived from slightly different data periods to prevent the hindcast-period wind information from entering into the hindcast experiments. An understanding of the behavior of coupled simulations obtained by the use of different SVD modes calculated from different data periods thus becomes necessary before proceeding to the hindcast experiments.

The SVD model is calculated from the co-variance matrix of observed SST anomaly and FSU wind stress anomaly, including only interannual variability. The standard version (referred to as SVDstd) used in part I is estimated from the data of 1970 to 1988, for a total 19-year period. Three other SVD modes are estimated: SVD2 uses a longer data record, from 1970 to 1993 (24-year record); SVD3 uses the same period as SVDstd, but excludes the two-year record of 1982 and 1983 in both SST and wind stress fields before calculating the co-variance matrix; SVD4 is the same as SVD3, but excludes different two-year records (1986 and 1987) before calculating the co-variance. Figures 1–4 show the time-longitude SST and zonal wind stress fields of 15-year coupled simulations for the four SVD models discussed, with their respective mean seasonal cycle removed. Except for the change of SVD modes, the HCM used in the coupled simulations is the same as the standard version described in part I, with the presence of the seasonal cycle. Compared with the results from SVDstd (Fig. 1), weaker oscillations are obtained for SVD2 (Fig. 2) and SVD3 (Fig. 3) and stronger oscillations are obtained for SVD4 (Fig. 4). The inclusion of the data of 1982–83 period, a very large ENSO event, seems to increase the amplitudes of the coupled oscillation. When the 1982–83 data is excluded (SVD3) or averaged out to a larger degree (SVD2), the coupled simulations show a weaker amplitude than the standard case. The SVD3 case shows an especially weak oscillation, of which the strength is about one quarter or less of that with the SVDstd model. However, excluding other ENSO events, such as 1986–87 (SVD4), does not create the same weakening effect. With SVD4, a stronger amplitude is obtained relative to the standard case. Although the coupled oscillation becomes stronger or weaker with different estimates of the SVD modes, the coupled periods are not significantly changed. For example, with SVDstd, the coupled interannual variability shows periods of 4-, 3- and 4-year from peak to peak in the 15-year simulation; with SVD2, the periods are 3.5, 3.5 and 4 years; with SVD3, a regular 3-year peak to peak period is obtained; a 4-year period is obtained with SVD4. All cases with the similar level of amplitudes (i.e., the SVDstd, SVD2 and SVD4) show an average period around 4 years. Even though SVD3 has a very weak amplitude, implying weak coupling strength between the ocean and atmosphere, the period is only slightly shorter than the other three. The periods of interannual variability do not seem as sensitive to the change of SVD modes as the amplitudes are. Spatial features are similar in all cases. For different modes, warm phases are locked to different months, although the latter half of a year is still preferred.

The change of amplitudes of coupled interannual variability for different SVD modes can be explained as the following: when different SVD modes are chosen, the atmospheric model behavior and also the coupling strength between the ocean and atmosphere are changed. The change of coupling strength can easily modify the amplitudes of the coupled oscillation, but does not have a strong impact on the frequency locking behavior (Jin et al. 1994, 1996; Syu et al. 1995). A set of experiments was carried out, in which the coupling coefficient was chosen to be larger or smaller than the standard value (1.0 in the standard version of HCM). It was found that the amplitudes of the ENSO oscillations can be adjusted

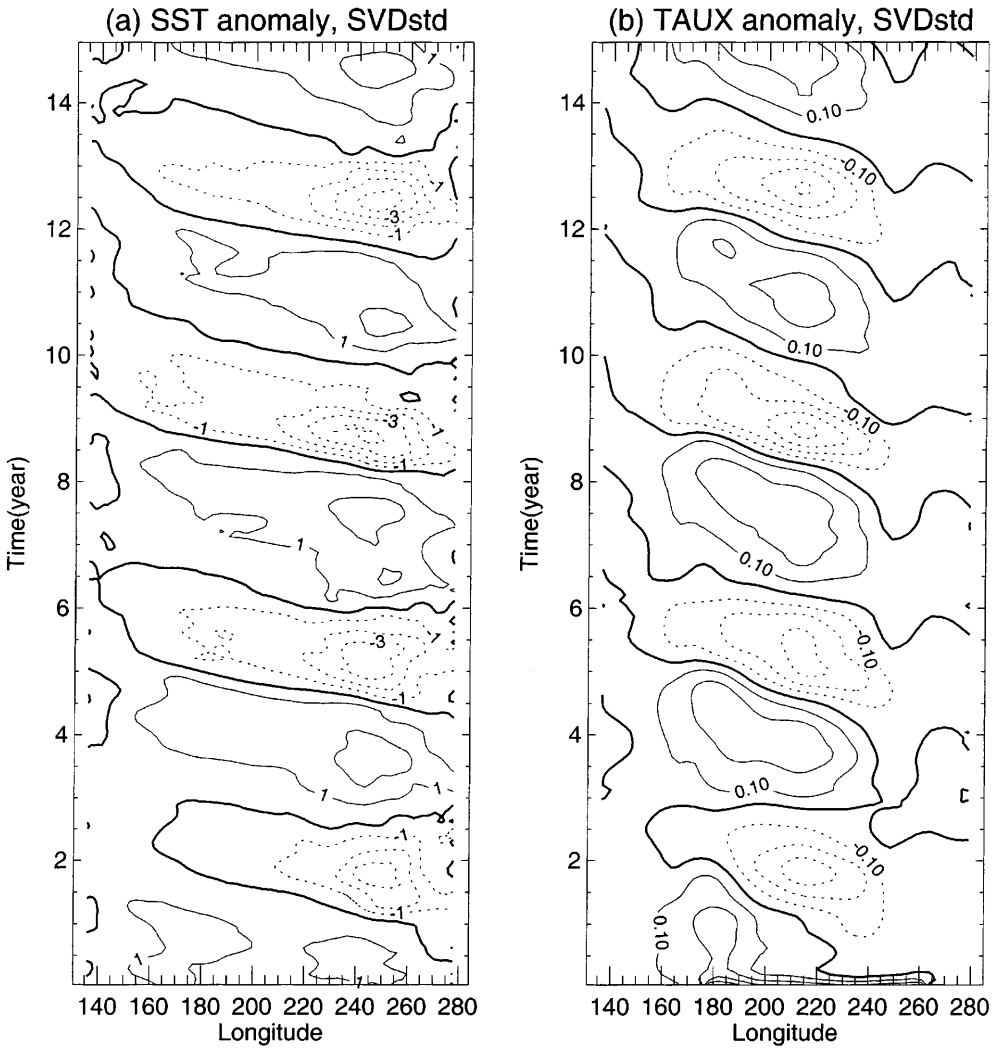

Fig. 1a, b Time-longitude distribution of **a** SST and **b** zonal wind stress anomaly fields, with respect to the mean seasonal cycle, for the coupled simulation with the SVDstd model (data period from 1970 to 1988 in calculating the SST-wind covariance matrix) in the presence of the seasonal cycle. Contour interval is 1 °C for SST anomalies and 0.1 dyne/cm^2 for wind stress anomalies. *Dashed lines* represent negative values

to the same level as the standard case simply by adjusting the coupling strength. For example, with a stronger coupling coefficient, 1.2 or 1.3, the coupled simulation (figure not shown) presents approximately the same level of coupled amplitudes as the SVDstd case with a coupling coefficient of 1.0. However, for some modes (e.g., SVD3), a very strong coupling coefficient (1.5) is necessary to fully recover the ENSO amplitudes to a comparable level with the SVDstd case. The large impact caused by the 82–83 ENSO case is again suggested.

Because an averaged quantity is used to derive the statistical SVD model, it was expected to exhibit less sensitivity to the choices of length and year of data record provided that the record is long enough. In other words, when a short period of data is withdrawn from the total record, only a small impact on the model should result. These sensitivity tests indicate that 19 years is not a long enough time series to avoid such sensitivity. Fortunately, coupled periods are far less sensitive than coupled amplitudes. Since the consistency of the coupled period is more important than the amplitude to ensure the performance of forecast experiments, and since for short-time integrations (such as 2-year hindcast runs), the sensitivity of SVD modes does not become significant, a set of re-estimated SVD modes for different forecast periods is considered appropriate to use in hindcast experiments.

4 Initial fields

The initial SST anomaly fields for the stress-only scheme, the injection scheme and the stress-from-SST scheme are shown in Fig. 5 as NINO3 indices for the period of 1978–93 (1980–93 for the injection scheme), along with the observed NINO3 SST anomalies. The month-to-month correlation between the initialization fields and observations are 0.71 for the stress-only scheme and 0.92 for the injection scheme. While both initialization schemes capture major observed ENSO events, the injection scheme captures the temporal phase in more detail than the stress-only scheme. The higher correlation obtained from the injection scheme is mainly due to the more realistic phase relationship compared

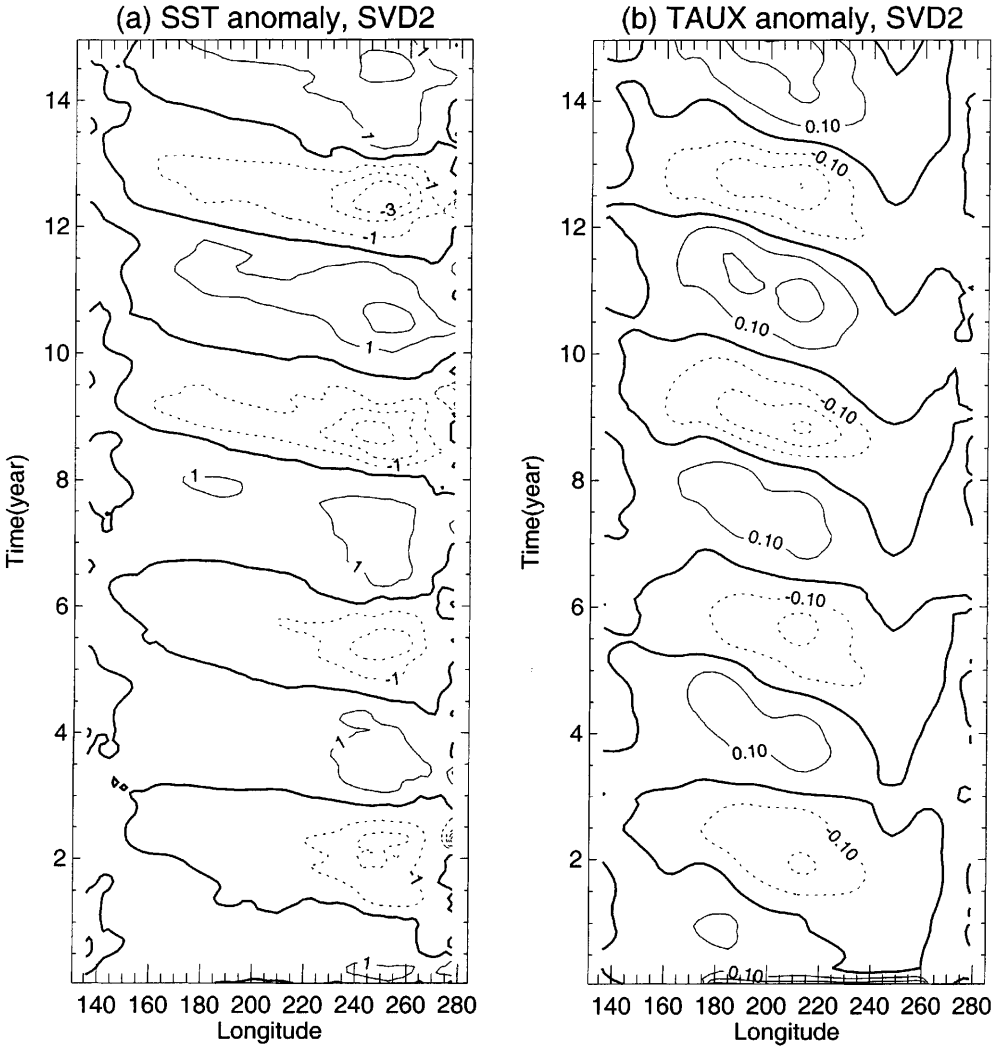

Fig. 2a, b Same as in Fig. 1, but for SVD2 model (data record of 1970 to 1993)

with the observations. The correlation of the stress-from-SST scheme is slightly higher than the stress-only case (0.74 versus 0.71), while the root mean square (RMS) error is slightly lower than the stress-only case (0.58 °C versus 0.60 °C). The slightly higher correlation in the stress-from-SST scheme indicates that the positive impact of observations of the actual weather time series and the negative impact of errors contained in the observed wind data set have an approximately equal but opposite effect in reproducing ENSO variability.

The inject-SST initialization scheme yields the highest correlation among all schemes, 0.997 (figure not shown, RMS error = 0.062 °C), as a result of being constrained to closely follow the observed SST anomaly.

4.1 Contribution of data assimilation schemes to ocean sub-surface structure

The upper-ocean thermal structures (represented by heat content anomaly field) for the CPC reanalysis data, the stress-only scheme, the injection scheme, and the inject-SST scheme are displayed in Fig. 6a–d for the period of 1980–1993 as a function of time and longitude along the equator. The upper-ocean thermal structure for the injection case exhibits greater resemblance to the CPC reanalysis data than either the stress-only or the inject-SST initial fields, while the stress-only and the inject-SST cases are very similar to each other. In particular, the warm anomaly in the western Pacific during 1980 seen in the CPC reanalysis data is captured in the injection case, but is absent in both the stress-only and inject-SST heat content fields. Also, the cold anomalies during 1985–86 in the eastern Pacific seen in the CPC reanalysis data and the injection case are missing in both the stress-only and inject-SST cases. Recalling that the inject-SST case has wind information as well as SST information, we note that little is gained by using both in terms of correcting the ocean sub-surface structure. The injection method, though sub-optimal, does help to correct subsurface structure against errors in observed wind.

4.2 Contribution of wind-feedback versus weather noise to ocean initial conditions

The observed wind field includes a part which is associated with SST fluctuations, i.e., directly associated

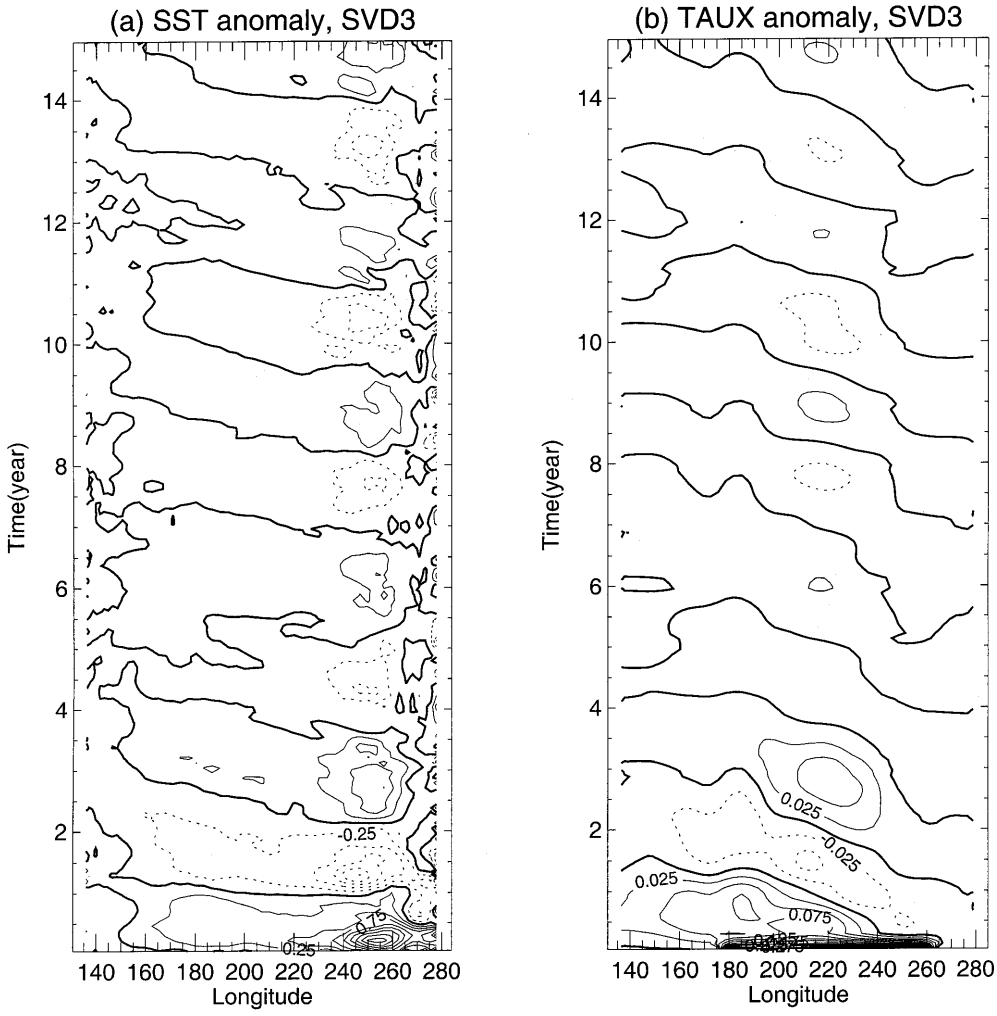

Fig. 3a, b Same as in Fig. 1, but for SVD3 model (data record of 1970–1981 and 1984–1988). Contour interval for this case is 0.25 °C for SST anomaly and 0.025 dyne/cm^2

with coupling, and a part which is independent atmospheric variability. To estimate how much information we can get from SST alone from a given atmospheric model, we consider the ocean sub-surface structure of the stress-from-SST run (Fig. 7a), in which the ocean was forced by wind stress which is output from the atmospheric model forced by the observed SST information. We compare this with the CPC analysis and the run forced by FSU wind (Fig. 6a, c). The heat content anomaly of the stress-from-SST case captures all basic characteristics, both phase and amplitude, presented in CPC analysis and the case with the stress-only scheme before 1990. For some years, e.g., 1984–1985, the heat content anomaly with the stress-from-SST scheme is actually closer to the CPC analysis than that given by the stress-only scheme which has a spurious short warm event during the cold phase in the eastern Pacific. However, from 1990 to 1993, although the overall pattern is captured, the amplitude of the heat content anomalies for the stress-from-SST case is much weaker than both the CPC reanalysis and the stress-only case.

As discussed in Sect. 2, we want to determine whether the constructive effect resulting from time history of observed weather noise on the ENSO mode is able to overcome the destructive effect resulting from errors contained in the observations. To do this, we separate the observed wind into two parts, the reconstructed winds, representing the wind-feedback given by the ocean SST, and the residual winds. Figure 7b shows heat content anomalies from a run forced by the residual winds. Figure 7c shows heat content anomalies obtained by subtracting those of the stress-from-SST (Fig. 7a) from the observed wind case (Fig. 6c). To the extent that Fig. 7c resembles Fig. 7b, it indicates that the OGCM response is approximately linear for this quantity. Although the OGCM includes full nonlinearity, the near-linearity shown by this comparison suggests we can separate the effects of the two wind-stress components. The effects of wind-feedback and weather noise on the ocean initial conditions, the only real-time information used in ENSO predictions, can thus be largely separated.

The correlation of the initial SST anomalies by using the residual wind with the observations is 0.14 (RMS error = 1.0 °C). This is significantly lower than the correlation of 0.74 given by the wind-feedback (stress-from-SST) case. Overall, the stress-from-SST case is capturing most of the ENSO signal, while the residual wind contributes a nosier signal with shorter time scales,

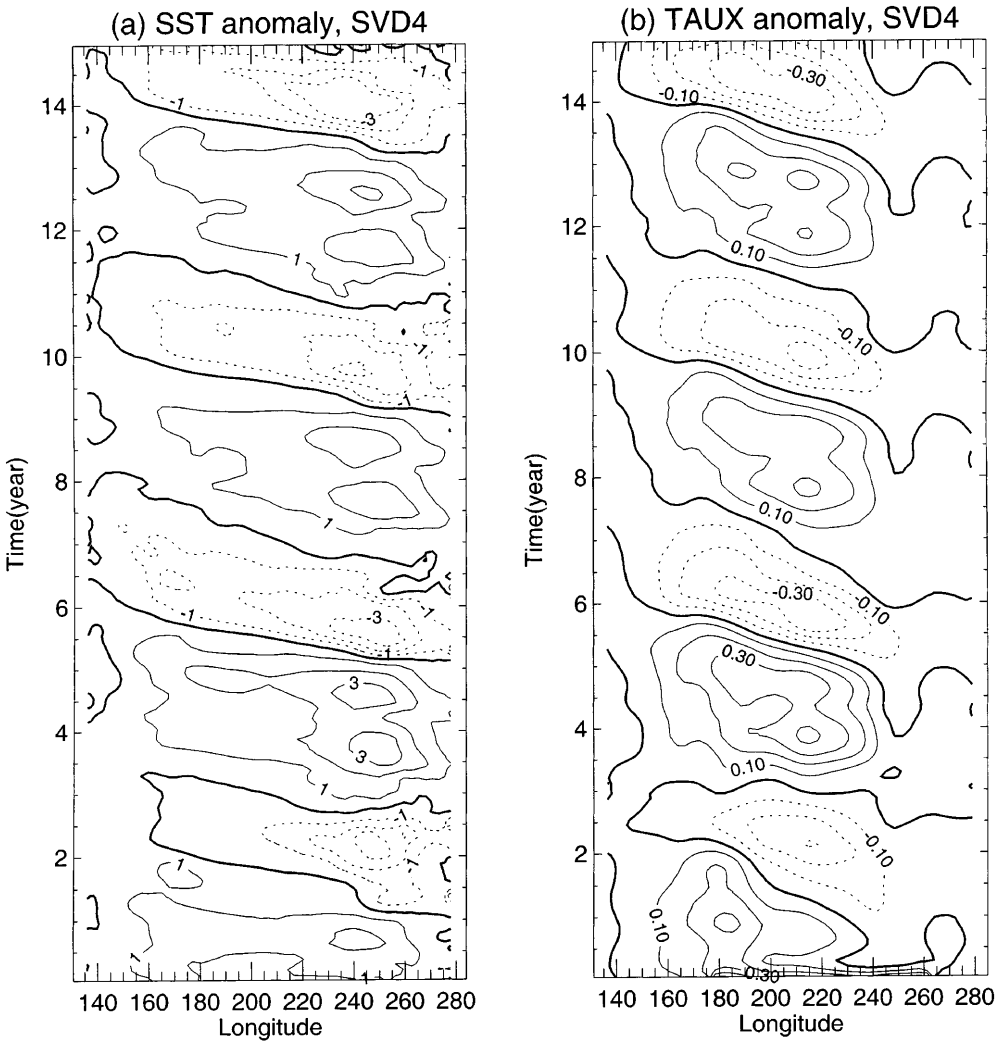

Fig. 4a, b Same as in Fig. 1, but for SVD4 model (data record of 1970–1985 and 1988)

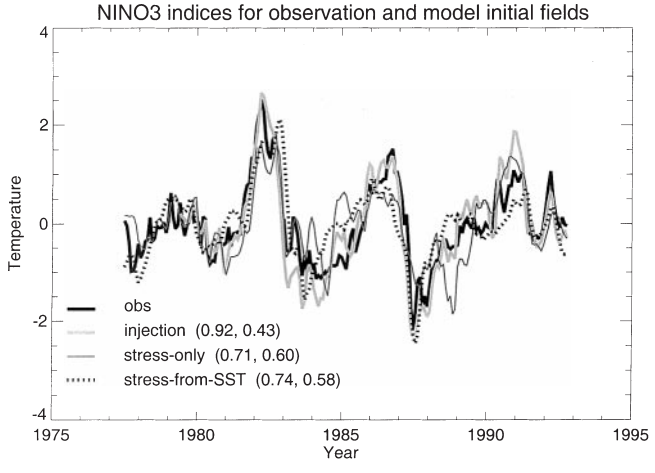

Fig. 5 Nino3 indices for observation and model initial fields with different initialization schemes. Month-to-month Correlation (the *first number*) and RMS error (the *second number*) between each model initial field and the observation are listed in *brackets*

that does not appear to have an obvious relation to the ENSO cycle. Although this is based on ocean model response rather than coupled response, it appears to indicate a dominance of the slow ENSO mode (involving the component of wind that depends on SST) over direct response to atmospheric uncoupled variability.

5 Prediction skill and discussion

We define the "standard" hindcast version as the hindcast experiments using a set of re-estimated SVD models in which no hindcast-period data have entered. In parallel, several hindcast experiments were conducted using the standard SVD model, as described in Sect. 3 (SVDstd), including data records overlapped with the hindcast period. This is referred to as the "dependent" hindcast version, because the hindcast results are no longer "independent" from the observations for the same period. Although the dependent version cannot be used for real prediction purposes because it is difficult to separate the artificial skill entered through observations in SVD modes, it can be used to estimate the performance of the hindcast model, as discussed in Barnett et al. (1993). We use dependent hindcast version results only for some comparison experiments.

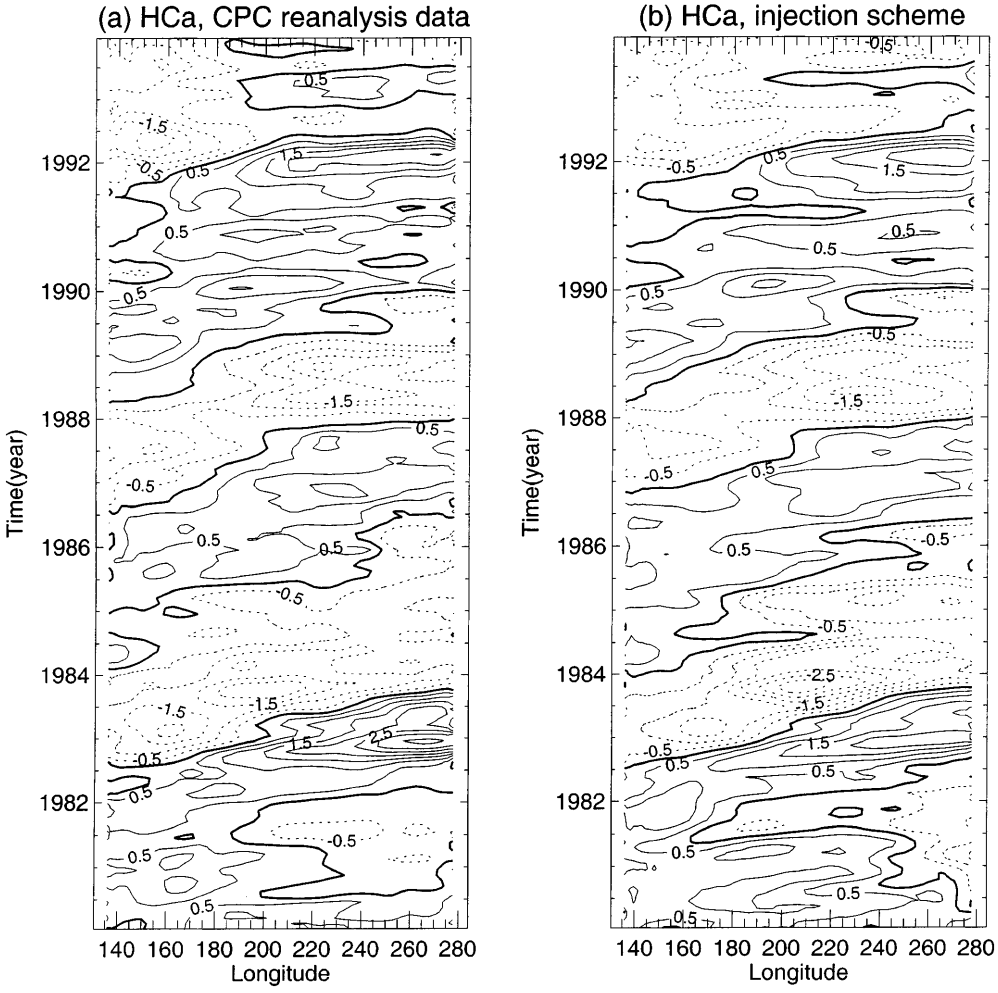

Fig. 6a–d Heat content anomaly fields of **a** CPC analysis data, and model initial fields **b** with the injection scheme **c** with the stress-only scheme, and **d** with the inject-SST scheme, as a function of time and longitude along the equator

Correlations and RMS errors for the period from 1980 to 1992 are calculated, with a total of 156 ensembles for the stress-only initialization and 155 for injection initialization. These correlation skills are computed from NINO3 index as a function of lead time, defined as the model time span from the beginning of the hindcast integration. A three-month running mean is applied, and the mean of each set of data for the same lead month is removed before calculating the correlations and RMS errors for all hindcast cases. The same procedures are also applied to the observed SST anomalies. Although removing the mean hindcast results before comparing the predicted anomalous SST is a technique commonly used in the ENSO prediction community and it is reasonable in the statistical sense, the real model behavior can not be evaluated unless the mean anomalies removed are also displayed. Figure 8 displays the mean SST anomalies, as a function of lead month, for observations, the case with the injection scheme and the case with the stress-only scheme, respectively. The mean SST anomalies for both initialization schemes show an increase at longer lead months, while the same quantity for observation has a near-zero value throughout the 2-year period. The stress-only scheme gives a larger drift than the injection scheme does. The drift reaches the saturation level within the hindcast period, around lead month 15 for the stress-only scheme and around lead month 20 for the injection scheme. The reason for the drift with both initialization schemes is thought to be related to our flux-correction procedure. However, the exact cause is not yet clear.

The results for both the stress-only initialization (dotted line) and the injection scheme (thin solid line) are shown in Fig. 9 as a function of lead month. The result of the dependent version for the injection initialization is also displayed in the same figure (gray line). Without correction by the observed ocean thermal information, the stress-only scheme gives a lower correlation initially, compared to the injection scheme, which is initially not far from the persistence (thick solid line) but starts to beat persistence after a lead time of 3 months. With the stress-only initialization (and with the standard hindcast version), the correlation starts from 0.75 and remains greater than 0.5 up to a lead time of 8 months with the RMS errors remaining lower than 1 °C over the entire hindcast period. With the injection initialization scheme and the standard hindcast version, the hindcast skill is improved–starting high at 0.94 and keeping at over 0.5 up to a lead time of 17 months. The improved ocean initial field becomes more prominent on longer lead

Fig. 6a–d (Contd.)

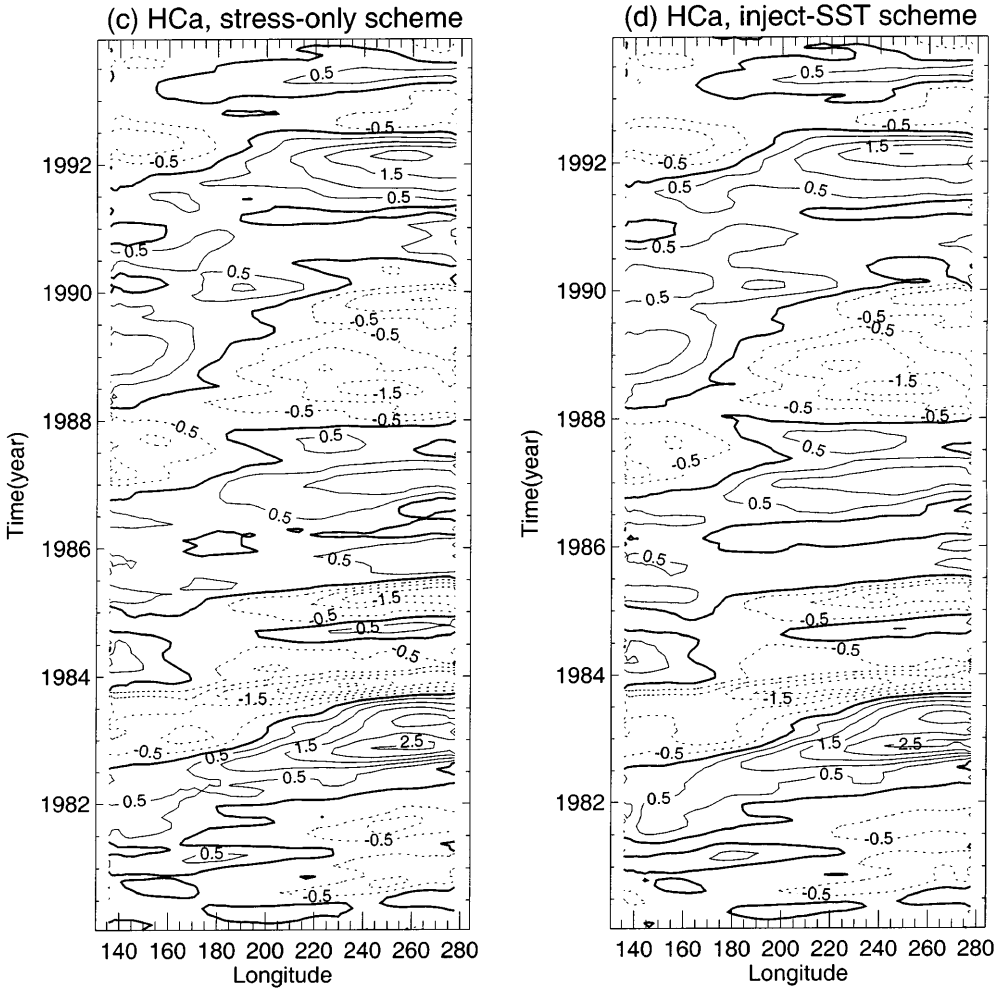

time. The overall correlation skill with the injection initialization scheme is approximately 0.1 to 0.2 higher than that with the stress-only initialization scheme.

The predicted and observed NINO3 indices, as a function of year, are displayed in Fig. 10, at the lead times of 0, 3, 6, 9, 12, 15, 18 and 21 months. Lead month 0 indicates the control run. Each vertical bar indicates one RMS error on both the positive and negative side of the predicted SST field. In general, the predicted SST field is able to capture the variation of the observed SST field though with less skill beyond 12 month lead. The La Niña events (1984–85, 1989) are better predicted than the El Niño events. For example, the enormous 1982–83 El Niño is not well predicted after lead month 9. In addition, although the warming trend in the 1990s is well predicted at all lead months, the small warm event during 1993 is not predicted at lead months 9, 12 and 15. This result is competitive with other prediction results as seen, e.g., in the review paper (Latif et al. 1998).

The dependent hindcast version in Fig. 9 (gray line), which allows the hindcast-period data to enter the hindcast run through the SVD model, shows approximately the same skill correlation with the standard hindcast version for the first 12 lead months and shows slightly higher (less than 0.1) correlation at longer lead times. In other words, the artificial skill introduced through the SVD model does not seem to be significant. Since the dependent version is the simplest hindcast experiment to set up, several other hindcast experiments using this version are also conducted (Figs. 11 and 12), but only for the purpose of sensitivity study in testing different initialization methods. The comparison among these dependent-version hindcast experiments thus represents the relative performance of each initialization scheme.

Figure 11 shows the comparison between the stress-only and stress-from-SST schemes, with the dependent hindcast version. The hindcast correlation by using the stress-from-SST scheme is slightly higher than that with the stress-only scheme. The RMS errors for both schemes, after the mean is removed at each lead month, are about the same in magnitude. Without the mean removed (figure not shown), the RMS error for the stress-from-SST scheme exhibits more conservative error growth than the stress-only scheme. While information in residual wind might be thought important, clearly its positive impact is smaller than the error effect. This suggests that the direct inclusion of stress due to specific

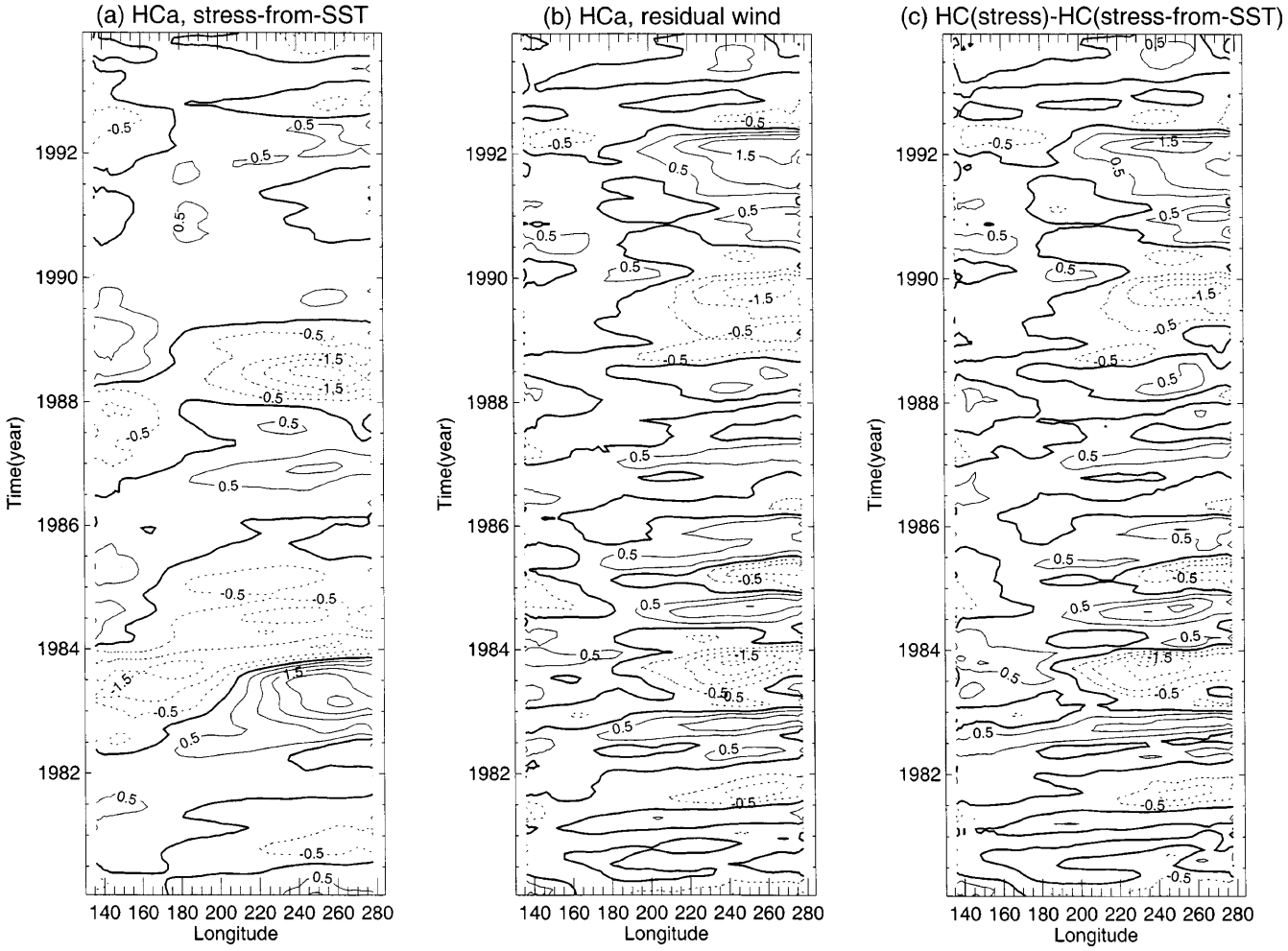

Fig. 7a–c Heat content anomalies calculated **a** for the case forced by SVD reconstructed wind; **b** for the case forced by residual wind (FSU wind minus SVD reconstructed wind); **c** as the departure of the case forced by FSU wind from that forced by SVD reconstructed wind

atmospheric events, such as westerly wind bursts, is not directly crucial to prediction, at least at the current level of skill.

To evaluate the impact given by the ocean sub-surface information in the initial field, we compared the hindcast skill of both the inject-SST scheme (black curve in Fig. 12) and the injection scheme (gray curve in Fig. 9), both with the dependent hindcast version. The inject-SST scheme gives a correlation nearly the same as the persistence at lead month 0, but drops quickly over a short lead time, although it finally rises at longer lead time. This seems counter-intuitive since the model has stress information as well as SST information, and yet fares worse in months 5–15 than the stress-only scheme. As discussed, using SST information to obtain wind stress, without modifying OGCM SST, performs rather well. Therefore, we hypothesize that the initial conditions provide a better projection on the model ENSO mode when OGCM SST is used than when the model is constrained to have observed SST. The improved initial SST is primarily projecting on model modes that decay over the first few months, typical of surface-layer processes.

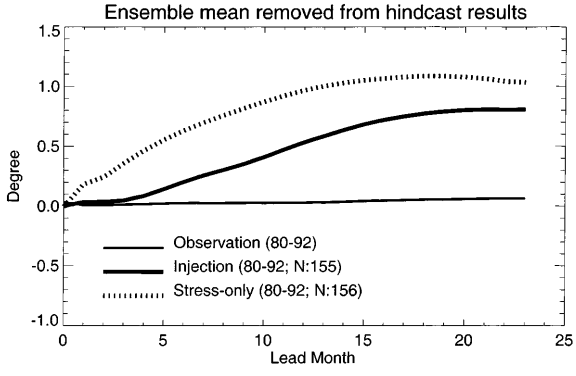

Fig. 8 Ensemble mean for each lead month removed in computing hindcast correlation and RMS error of NINO3 SST anomalies for observations (*thin solid line*), the hindcast results with the injection scheme (*thick solid line*) and the hindcast results with the stress-only scheme (*dotted line*). A three-month running average is applied in original data set before calculating the mean

Chen et al. (1995), using the CZ model and an initialization scheme in which the initial ocean field is forced by observed wind stress blended with wind stress

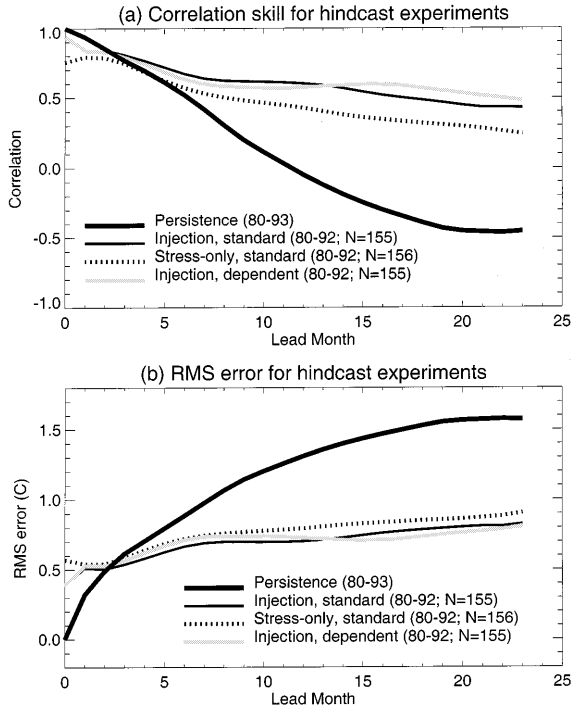

Fig. 9 **a** Correlation skills and **b** RMS errors for the standard (*thin solid line*) and dependent (*gray line*) hindcast experiments with the injection scheme, and the standard version with the stress-only scheme (*dotted line*). A three-month running mean is applied and the ensemble mean for each lead month (e.g., values shown in Fig. 8 for the standard experiments and observations) is removed in both the observation and model results before calculation

produced by the coupled model within a narrow equatorial band between 7°S and 7°N (referred to as "nudged-wind" scheme), obtained a much improved correlation skill. Hindcasting from 1972–92, their correlation is greater than 0.6 up to 20-month lead time. However, a much lower correlation skill is obtained when the nudged-wind scheme is applied in the HCM (gray curve in Fig. 12). In our HCM, the wind field given by the empirical atmospheric model is realistic. The nudged-wind scheme in fact results in greater initial error from the ocean model in the HCM. The wind field produced by the CZ model has considerable mismatch with data, thus resulting in a degraded heat content field compared to the original initialization scheme in Cane et al. (1986) (Perigaud et al. submitted 1999). Thus for the CZ model, a better projection on the ENSO mode can apparently be obtained by introducing compatible errors in the initial conditions. In addition, the Chen et al. (1995) nudged-wind scheme used some tunable parameters as the weighting for the observed wind and model produced wind. These "nudging parameters" were chosen experimentally to give good predictions over the hindcast cases. While this scheme shows indications of success in improving hindcast skill for the CZ model, whether this scheme can be generalized remains an open question. Our results suggest it is less beneficial if the model atmospheric response is realistic.

Predictions after 1992 with the injection scheme are made using the HCM. Figure 13 presents the predicted NINO3 indices, at 3-, 6- and 9-month lead, from 1993–1999. Observations through February 1999 are used. Averages of each lead month based on forecast verification over the period of 1980–1992 (Fig. 8) are removed. Vertical bars represent plus and minus one RMS error, over the same forecast verification time span. For all lead months shown here, the predicted SST variations in the early 1990s tend to be colder and have stronger amplitudes than observed. The predicted warm events for all lead times shown here appear to have a delay time of several months compared with observations. The forecast does predict the warm event of 1997/98, although with a more moderate amplitude and with considerable delay, especially at 9-month lead time. The rapid transition to the subsequent cold event is reasonably well predicted.

6 Conclusions

Using the hybrid coupled model described in part I of this two-part study, the performance of ENSO predictions is examined in part II. The HCM incorporates a surface-layer mixing parametrization in addition to the modified Richardson-number-dependent vertical mixing scheme in the oceanic component, and a simple parametrization of atmospheric spin-up time. The simulated ENSO oscillations using the standard version of the HCM have reasonable spatial and temporal structures as well as realistic interannual periods (3 to 4 years).

Before proceeding to ENSO hindcast experiments, a set of SVD models are re-estimated to avoid using observations that overlap with the hindcast period. Although a noticeable sensitivity is seen in the simulated ENSO cycles using slightly shorter or longer data period in estimating the SVD model, the coupled period is less sensitive and the first two-year integrations do not differ significantly. The re-estimated SVD model is thus considered suitable for ENSO prediction purposes.

The ENSO prediction experiments include four initialization schemes: the standard Cane et al. (1986) initialization scheme, in which the ocean is forced by observed wind stress (stress-only); a piggyback scheme, in which the CPC data assimilation product (obtained from a model close to ours) is injected into the ocean initial field once a month (injection) in addition to observed wind stress forcing; the wind-from-SST scheme, in which the ocean model is initiated by SVD model derived winds from observed SST; and the inject-SST scheme in which, in addition to wind stress, only SST information is injected into the model. With the injection scheme, the HCM obtains a much improved hindcast skill compared to the stress-only scheme, especially at longer lead times, and is competitive with other prediction models. NINO3 correlation exceeds 0.5 up to a lead time of 17 months. Using the CPC data assimilation product, at cheaper cost, instead of developing our own

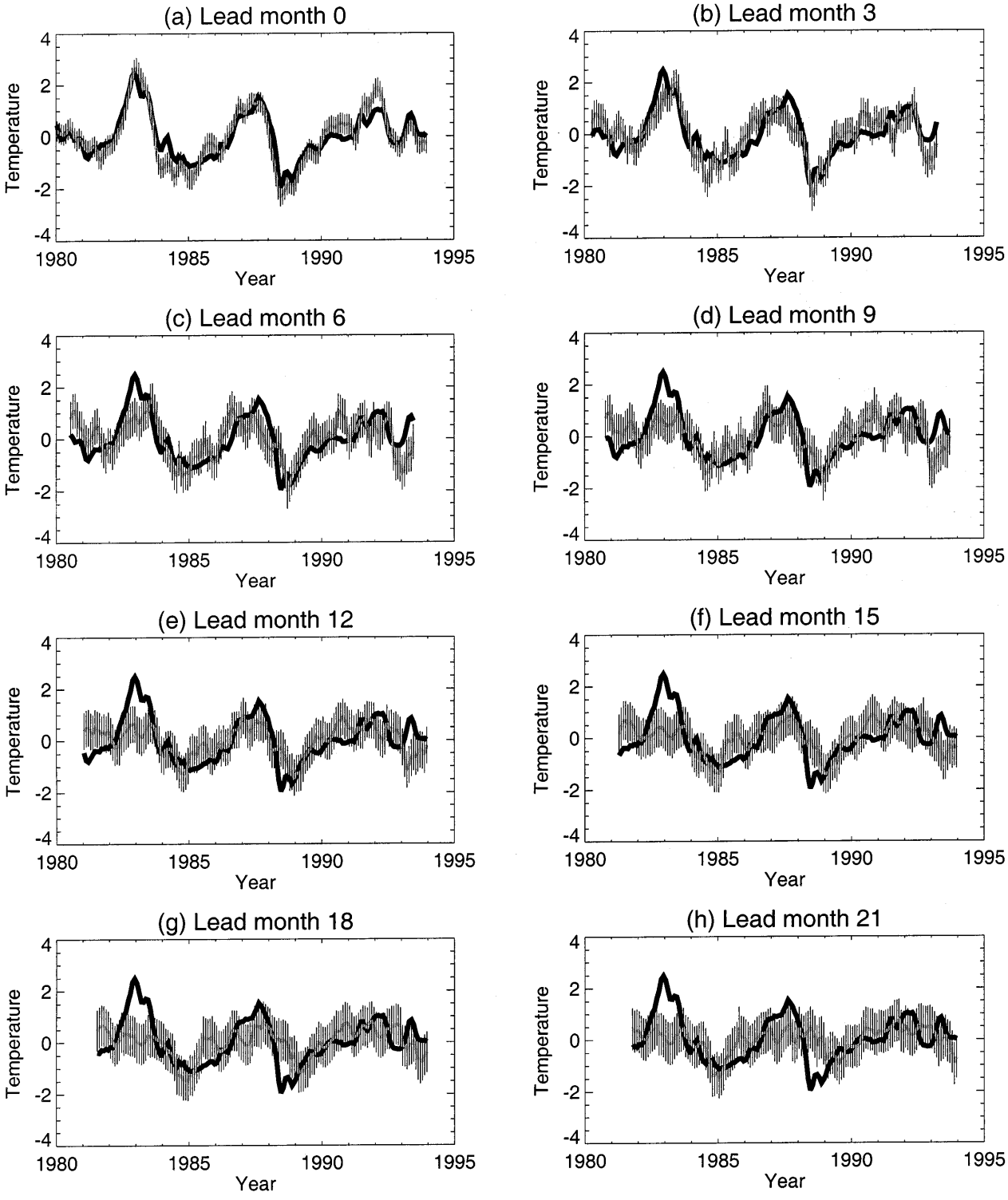

Fig. 10a–h Hindcasts of the NINO3 SST anomaly using the standard hindcast version and injection scheme for **a** 0, **b** 3, **c** 6, **d** 9, **e** 12, **f** 15, **g** 18, and **h** 21 lead months. The *vertical bars* show plus and minus one RMS error. The *black solid line* indicates the observed SST anomalies and the *gray solid line* indicates the predicted SST anomalies. The hindcast period is from February 1980 to December 1992, for an ensemble of 155 forecasts

data assimilation scheme is shown to work well. This suggests that not every model needs to have its own data assimilation scheme, provided the data assimilation product is chosen properly.

The importance of upper-ocean thermal structure is demonstrated by comparing the results with the injection scheme and the inject-SST scheme. The inject-SST scheme, in which the observed SST is applied to the

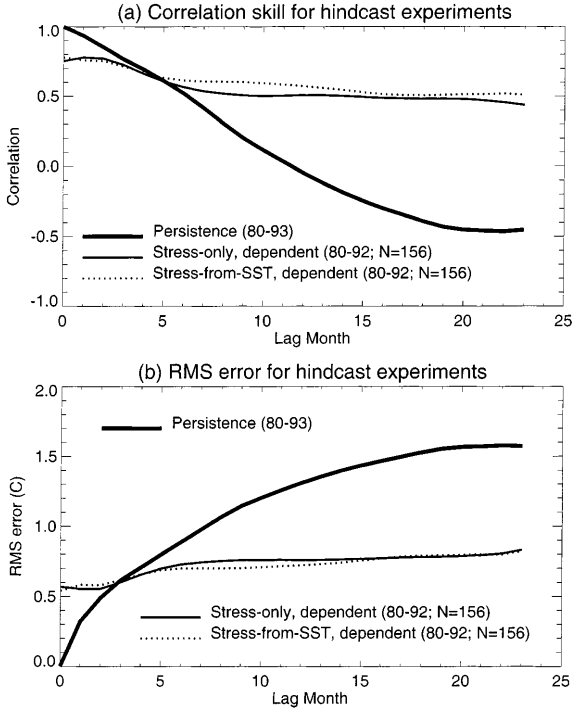

Fig. 11 **a** Correlation skills and **b** RMS errors for the dependent hindcast experiments with the stress-only scheme (*thin solid curve*) and the stress-from-SST scheme (*dotted line*). The same calculation method as in Fig. 9 is applied

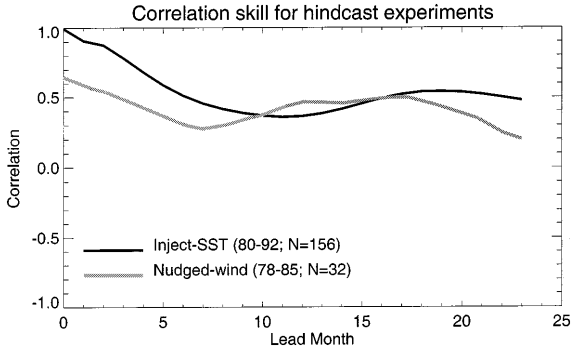

Fig. 12 Correlation skills for the dependent hindcast experiments with the inject-SST scheme (*black curve*) and the nudged-wind scheme (*gray curve*). The inject-SST scheme has an ensemble of 156 forecasts from 1980 to 1992. The nudged-wind scheme has a smaller ensemble of 32 forecasts from 1978 to 1985 only. The same calculation method as in Fig. 9 is applied for both schemes

model daily, gives a high correlation initially but drops quickly over a short lead time: starting from lead month 3, the correlation of the inject-SST scheme drops lower than that of the injection scheme. In addition, although it has both stress and SST information, the inject-SST scheme does not perform better than the stress-only scheme or the stress-from SST scheme. This suggests that the initial conditions provide a better projection on the model ENSO mode when OGCM SST is used than when the model is constrained to have observed SST.

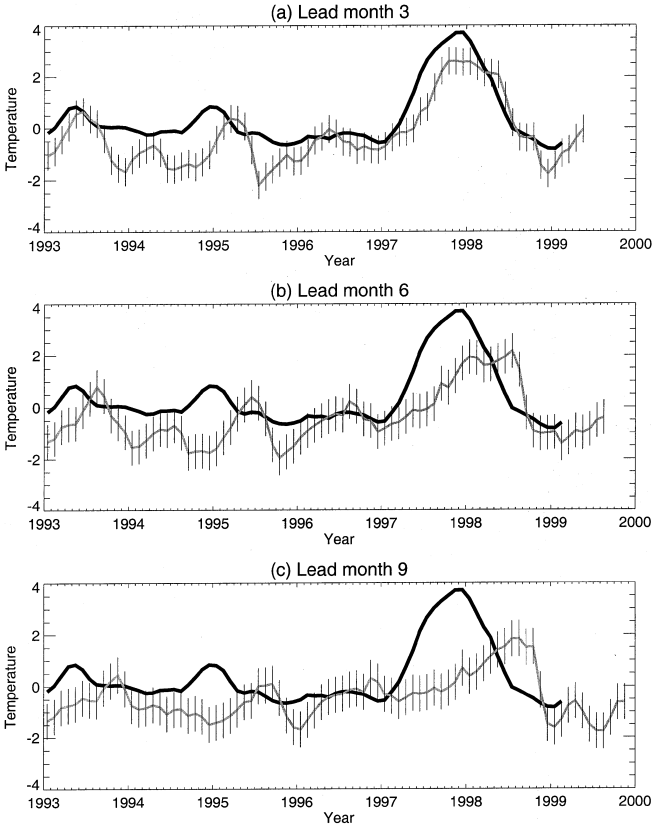

Fig. 13a–c Forecasts of NINO3 SST anomalies from 1993 to 1999 (the latest forecast starts from February 1999). The *solid line* indicates observations. The mean for each lead month over the forecast verification time span (1980–1992) is removed (see Fig. 8). *Vertical bars* represent plus and minus one RMS error as in Fig. 10. **a** 3-month, **b** 6-month and **c** 9-month lead

By comparing the stress-only and stress-from-SST schemes, the effects of the wind component associated with SST variations and the wind component due to weather noise plus observation error can be separated. Both schemes show the same level of hindcast skill, indicating that the wind component associated with the slow ENSO mode is crucial for the prediction problem. This result also implies that information about the past history of the weather noise is not able to overcome the additional errors contained in the current wind stress observations to improve forecast skill. Presumably accurate observations of atmospheric internal variability can help in ENSO prediction, but it appears that most current skill is contained within the coupled ENSO mode.

Acknowledgements This work was supported in part by National Oceanography and Atmosphere Administration grant NA56GP0451 and NA86GP0314, and National Science Foundation grant ATM-9521389. Computations were carried out at the Florida State University Computer Center, sponsored by the NOAA climate and global change program. We thank M. Ji and A. Leetmaa of the NOAA Climate Prediction Center (CPC) for providing the ocean reanalysis data, D. Gutzler for providing the SVD code, W. Weibel for computing assistance and C. Perigaud for discussions. We also thank Dr. Lee-Lueng Fu at the Jet Propulsion

Laboratory/California Institute of Technology for supporting HHS in finishing this paper at JPL. Figure 13 has previously appeared in the Experimental Long-Lead Forecast Bulletin, formerly distributed by CPC and now by the Center for Ocean-Land-Atmosphere Studies.

References

Barnett TP, Latif M, Graham N, Flügel M, Pazan S, White W (1993) ENSO and ENSO-related predictability. Part I: prediction of equatorial Pacific sea surface temperature with a hybrid coupled ocean-atmosphere model. J Clim 6: 1545–1566

Barnston AG, Ropelewski CF (1992) Prediction of ENSO episodes using canonical correlation analysis. J Clim 5: 1316–1345

Blanke B, Neelin JD, Dutzler D (1997) Estimating the effect of stochastic wind stress forcing on ENSO irregularity. J Clim 10: 1473–1485

Blumenthal MB (1991) Predictability of a coupled ocean-atmosphere model. J Clim 4: 766–784

Cane MA, Zebiak SE (1985) A theory for El Niño and the Southern Oscillation. Science 228: 1084–1087

Cane MA, Zebiak SE (1987) Prediction of ENSO events in a physical model. In: Cattle H (ed) Atmospheric and Oceanic Variability, Royal Meteorological Society Press, Bracknell, Berkshire pp 153–182

Cane MA, Sarachik ES, Dolan SC (1986) Experimental forecasts of El Niño. Nature 321: 827–832

Chang P, Wang B, Li T, Ji L (1994) Interactions between the seasonal cycle and the Southern Oscillation–frequency entrainment and chaos in an intermediate coupled ocean-atmosphere model. Geophys Res Lett 21: 2817–2820

Chang P, Ji L, Wang B, Li T (1995) Interactions between the seasonal cycle and El Niño-Southern Oscillation in an intermediate coupled ocean-atmosphere model. J Atmos Sci 52: 2353–2372

Chen D, Zebiak SE, Busalacchi AJ, Cane MA (1995) An improved procedure for El Niño forecasting: implications for predictability. Science 269: 1699–1702

Eckert C, Latif M (1997) Predictability of a stochastically forced hybrid coupled model of the tropical Pacific ocean-atmosphere system. J Clim 10: 1488–1504

Fischer M, Latif M, Flügel M, Ji M (1995) On the benefit of sea level assimilation in the tropical Pacific. WMO/TD 651: 1–22

Hao Z, Ghil M (1994) Data assimilation in a simple tropical ocean model with wind-stress errors. J Phys Oceanogr 24: 2111–2128

Goswami BN, Shukla J (1991) Predictability of a coupled ocean-atmosphere model. J Clim 4: 3–22

Ji M, Leetmaa A (1997) Impact of data assimilation on ocean initialization and El Niño. Mon Weather Rev 125: 742–753

Ji M, Kumar A, Leetmaa A (1994) An experimental coupled forecast system at the National Meteorological Center. Some early results. Tellus 46A: 398–418

Ji M, Leetmaa A, Derber J (1995) An ocean analysis system for seasonal to interannual climate studies. Mon Weather Rev 123: 460–481

Ji M, Leetmaa A, Kousky VE (1996) Coupled model forecasts of ENSO during the 1980s and 1990s at the National Meteorological Center. J Clim 9: 3105–3120

Jiang N, Ghil M, Neelin JD (1995) Forecasts of Equatorial Pacific SST anomalies using an autoregressive process using singular spectrum analysis. Experimental Long-lead Forecast Bull 4(1): 24–27

Jin F-F, Neelin JD, Ghil M (1994) El Niño on the ''Devil's Staircase'': annual subharmonic frequency locking and ENSO aperiodicity. Science 264: 70–72

Jin F-F, Neelin JD, Ghil M (1996) El Niño/Southern Oscillation and the annual cycle: subharmonic frequency locking and aperiodicity. Physica D 98: 442–465

Kleeman R, Power SB (1994) Limits to predictability in a coupled ocean-atmosphere model due to atmospheric noise. Tellus 46A: 529–540

Kleeman R, Moore AM (1997) A theory for the limitation of ENSO predictability due to stochastic atmospheric transients. J Atmos Sci 54: 753–767

Latif M, Flügel M (1991) An investigation of short-range climate predictability in the tropical Pacific. J Geophys Res 96: 2661–2673

Latif M, Sterl A, Maier-Reimer E, Junge MM (1993) Structure and predictability of the El Niño/Southern Oscillation phenomenon in a coupled ocean-atmosphere general circulation model. J Clim 6: 700–708

Latif M, Anderson D, Barnett T, Cane MA, Kleeman R, Leetmaa A, O'Brien JJ, Rosati A, Schneider E (1998) TOGA review paper: ''Predictability and prediction.'' J Geophys Res 103: 14375–14393

Legler DM, O'Brien JJ (1984) Atlas of tropical Pacific wind stress climatology 1971–1980. Department of Meteorol, Florida State University, Tallahassee, Florida, 182pp

Penland C, Sardeshmukh PD (1995) The optimal growth of tropical sea surface temperature anomalies. J Clim 8: 1999–2024

Reynolds RW (1988) A real-time global sea surface temperature analysis. J Clim 1: 75–86

Rosati A, Miyakoda K, Gudgel R (1997) The impact of ocean initial conditions on ENSO forecasting with a coupled model. Mon Weather Rev 5: 754–772

Syu H-H, Neelin JD (1997) Prediction of NINO3 SST anomaly in a hybrid coupled model with piggy-back data assimilation. Experimental Long-lead Forecast Bull 6(3): 14–17

Syu H-H, Neelin JD (1999) ENSO in a hybrid coupled model. Part I: sensitivity to physical parametrizations. Clim Dym (in press)

Syu H-H, Neelin JD, Gutzler D (1995) Seasonal and interannual variability in a hybrid coupled GCM. J Clim 8: 2121–2143

Tziperman E, Stone L, Cane MA, Jarosh H (1994) El Niño chaos: overlapping of resonances between the seasonal cycle and the Pacific ocean-atmosphere oscillator. Science 246: 72–74

Tziperman E, Cane MA, Zebiak S (1995) Irregularity and locking to the seasonal cycle in an ENSO prediction model as explained by the quasi-periodicity route to chaos. J Atmos Sci 52: 293–306

Xu J-S, von Storch H (1990) Predicting the state of the Southern Oscillation using principal-oscillation-pattern analysis. J Clim 3: 1316–1329

Xue Y, Cane MA, Zebiak SE, Blumenthal B (1994) On the prediction of ENSO: a study with a low-order Markov model. Tellus 46A: 512–528